Available online at www.sciencedirect.com
ScienceDirect
Journal of the European Ceramic Society 31 (2011) 1873–1879
www.elsevier.com/locate/jeurceramsoc

Analysis of the isothermal crystallization of $CaSiO_3$ in a $CaO–Al_2O_3–SiO_2$ melt through *in situ* observations

J. Heulens *, B. Blanpain, N. Moelans

Department of Metallurgy and Materials Engineering, Katholieke Universiteit Leuven, Kasteelpark Arenberg 44 - box 2450, B-3001 Heverlee, Belgium

Received 9 February 2011; received in revised form 14 March 2011; accepted 20 March 2011
Available online 27 April 2011

Abstract

Crystal growth of Wollastonite ($CaO·SiO_2$) in a $42CaO–10Al_2O_3–48SiO_2$ melt is observed *in situ* at 1320 °C and 1370 °C using a high-temperature confocal scanning laser microscope (CSLM). The crystallization is initiated by seeding the melt with Wollastonite particles, which is the primary phase at these temperatures and composition. At 1370 °C, a faceted growth form is observed, while at 1320 °C, dendritic, non-faceted growth occurs. The dendrite tip velocity is measured and compared with Ivantsov's theory. The presented experimental technique proofs to be successful for characterizing isothermal crystallization of minerals in silicate melts.
© 2011 Elsevier Ltd. All rights reserved.

Keywords: Interfaces; Non-destructive evaluation; Diffusion; Silicate; Crystal growth

1. Introduction

Crystallization of silicate melts is a widely investigated phenomenon in application domains such as geology, pyrometallurgy and glass making. Silicate melts in geological research are mostly referred to as magma or lava and crystal growth in these melts controls many textural and chemical features of igneous rocks.[1] In high temperature metal extraction processes (pyrometallurgy), the silicate melt, resulting from the used ores, is called slag. Crystallization or solidification of such slags influences the behavior of freeze linings[2] of pyrometallurgical reactors, the mineralogy of the cooled slag after tapping[3] or the usability of mold fluxes during continuous casting of steel.[4] Moreover, the knowledge about crystallization of silicate melts is of great importance to the production of glass ceramics.[5]

High temperature crystallization processes can be observed *in situ* using a hot stage confocal laser microscope (CSLM).[6,7] This technique offers numerous advantages over classical experimental techniques, in which the sample is quenched after different times.[8] For example, several isothermal observations can be made in a single experiment and quenching effects, such as phase transformations during cooling, are avoided. Recently, the CSLM has been used to study the dissolution behavior of refractory particles in slags.[9,10,11,12] Furthermore, Orrling et al. investigated the crystallization of slags under a temperature gradient[13] and the effect of alumina particles on the crystallization behavior of $CaO–Al_2O_3–SiO_2–MgO$ slags.[4] In the latter system, alumina particles were added to the melt to decrease the required undercooling for crystallization.

In this work, the crystallization of a primary phase is observed *in situ* by seeding the supersaturated silicate melt with the primary phase itself. In contrast to adding oxide particles as nucleation sites,[4] intermediate reaction products between the nucleation site and the silicate melt are avoided, which allows a more straightforward interpretation and a more accurate analysis. The experimental dendrite growth conditions are compared with the 2D and 3D Ivantsov solution. Furthermore, the appropriate dimensionless numbers are calculated to validate the assumptions of an isothermal experiment and diffusion-controlled mass transport.

The remainder of this paper is structured as follows. The experimental setup and procedure is explained in Section 2 and the results are presented and discussed in Section 3. In Section 4, the conclusions are formulated.

* Corresponding author. Tel.: +32 16 32 17 81.
E-mail addresses: jeroen.heulens@mtm.kuleuven.be (J. Heulens), bart.blanpain@mtm.kuleuven.be (B. Blanpain), nele.moelans@mtm.kuleuven.be (N. Moelans).

0955-2219/$ – see front matter © 2011 Elsevier Ltd. All rights reserved.
doi:10.1016/j.jeurceramsoc.2011.03.038

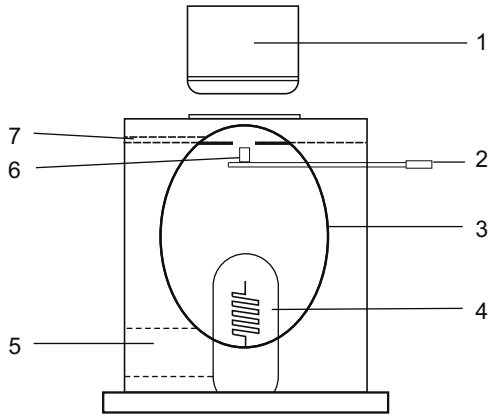

Fig. 1. Schematic representation of the high temperature CSLM technique: (1) objective lens of the laser microscope, (2) sample holder with thermocouple, (3) gold plated ellipsoidal chamber, (4) halogen lamp, (5) outlet to the vacuum system, (6) Platinum crucible with sample, (7) inlet for auxiliary gases.

2. Experimental technique

The crystallization experiments were done in an infrared (IR) heating chamber combined with a confocal scanning laser microscope (CSLM, Lasertec, 1LM21H-SVF17SP, Japan). A schematic of the equipment is shown in Fig. 1. The sample is heated by a 1.5 kW halogen lamp in a focal point of a gold plated ellipsoidal chamber while the sample is in the other focal point. This infrared heating system can reach temperatures up to 1700 °C in a few minutes. The sample temperature is measured with a B-type thermocouple at the bottom of the Platinum sample holder (see Fig. 4). The sample temperature is calibrated with the melting temperature of pure metals in Al_2O_3 crucibles: Cu (1085 °C), Ni (1453 °C), Fe (1538 °C) and Pd (1555 °C). The temperature in the crucible, at about 4–5 mm above the crucible bottom, is 30 ± 5 °C lower than the measurement of the thermocouple, as shown in Fig. 2. From this figure, it is clear that the offset on the calibrated temperature is constant over the temperature range under consideration. The CLSM chamber is flushed three times with purified Argon before it is filled with Argon at atmospheric pressure.

The silicate melt (slag) is prepared by mixing analytical grade powders of $CaCO_3$, Al_2O_3 and SiO_2 in the appropriate amounts and melting this mixture at 1600 °C for 2 h in a 50 cm^3 Platinum crucible to obtain a homogeneous melt with a composition of 42 wt% CaO, 10 wt% Al_2O_3 and 48 wt% SiO_2. The liquidus temperature of this composition is 1424 °C, as calculated with the FToxid database (version 2010) from FACTSage.[14] The composition lies in the primary phase region of Wollastonite, as shown in the phase diagram in Fig. 3. The melt is poured on a steel plate and crushed to particles of a few cubic millimeters. Several premelted glass particles are put in a Platinum crucible (5 mm diameter and 6 mm height) and placed on the sample holder of the CSLM chamber. This crucible is heated to 1600 °C at 200 °C min^{-1} and cooled down at the same rate to obtain a dense glass in the crucible, as indicated with [5] in Fig. 4.

Wollastonite ($CaO{\cdot}SiO_2$) is produced by premelting $CaCO_3$ and SiO_2 in the stoichiometric ratio in a 50 cm^3 Platinum crucible at 1640 °C (the melting point is 1544 °C). The melt

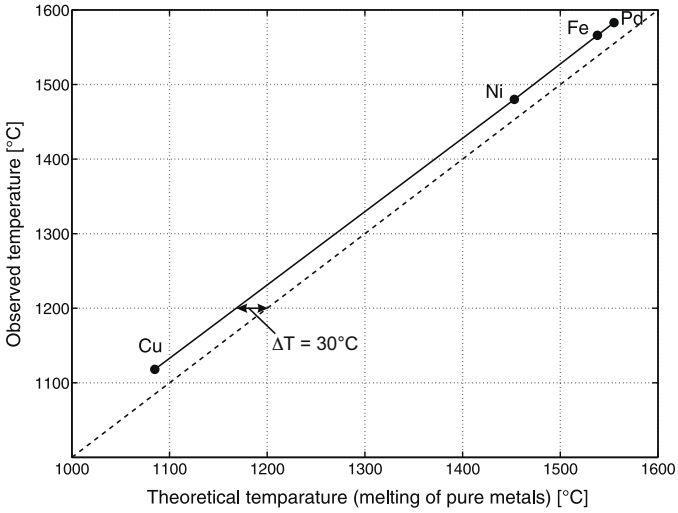

Fig. 2. Calibration of the observed temperature, measured with a B-type thermocouple at the bottom of the Platinum sample holder. This graph shows the observed temperature in comparison with the theoretical temperature, as determined from the melting temperature of respectively Cu (1085 °C), Ni (1453 °C), Fe (1538 °C) and Pd (1555 °C). The onset of melting of these metals was determined visually. The temperature in the crucible, at the plane of observation, is therefore 30 ± 5 °C lower than the measurement of the thermocouple.

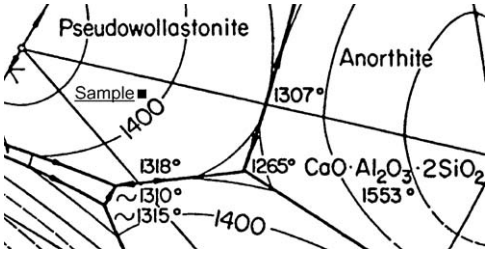

Fig. 3. Zoom-in of the $CaO–Al_2O_3–SiO_2$ liquidus projection.[22] The melt composition of this work is indicated with a black filled square. It is clear that this composition lies in the primary phase region of Wollastonite.

is slowly cooled at 0.1 °C min^{-1} to room temperature, which causes the melt to crystallize in long fiber crystals. The crucible content is crushed in a rotary mill to produce a fine powder of Wollastonite fibers (2–5 μm). The powder was identified as Wollastonite using XRD, for which the spectrum is shown in Fig. 5. At room temperature, a few of these fibers

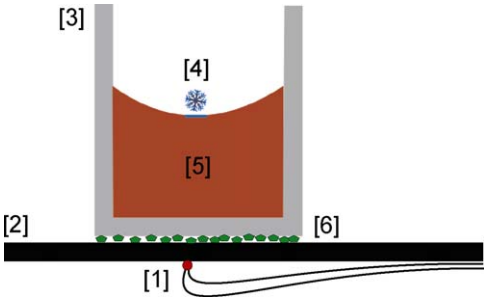

Fig. 4. Schematic drawing of the sample crucible: (1) Pt/Pt–10%Rh thermocouple, (2) Platinum sample holder, (3) Platinum crucible, (4) crystallizing Wollastonite, (5) bulk silicate melt, (6) Al_2O_3 powder to prevent welding of the Platinum parts.

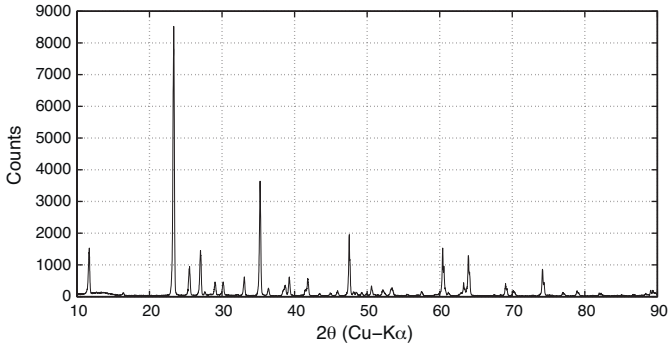

Fig. 5. XRD spectrum of the Wollastonite powder. All peaks are associated with the low-temperature polymorph α-Wollastonite, which has a triclinic crystal structure.[15]

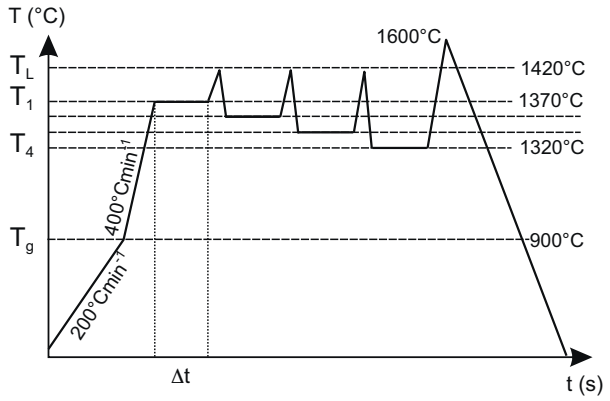

Fig. 7. Temperature profile of a single CSLM experiment to obtain growth morphologies and velocities at different isothermal sections. The sample is heated at 200 ° C min^{-1} and around the glass transition temperature, $T_g \approx 900$ °C, the heating rate is increased to 400 ° C min^{-1} to prevent full crystallization of the glass. After observation at a fixed temperature, $T_1 \ldots T_4$, for a certain time Δt, the crystals are remelted by heating to the liquidus temperature, $T_L = 1420$ °C, after which the sample is quenched to the next observation temperature. At the end of the experiment, the sample is heated to 1600 °C, to obtain a homogeneous melt, which is quenched to a glass at room temperature.

are put on top of the glass using fine tweezers. Fig. 6 shows a micrograph, from the laser microscope, of the Wollastonite fibers on the premelted glass, before starting the actual crystallization experiment. Wollastonite is the primary phase of crystallization for the melt, and, therefore, we expect the growing crystals to be Wollastonite. There is no thermodynamic driving force for other phases to form or grow in the temperature and composition range of the experiments. Furthermore, the nucleation barrier vanishes with the addition of Wollastonite to the melt.

The assembly of premelted glass with Wollastonite fibers on top, illustrated in Fig. 4, is subjected to a temperature profile, which is shown in Fig. 7. The sample is heated at 200 ° C min^{-1} and around the glass transition temperature (±900 °C) the heating rate is increased to 400 ° C min^{-1} to prevent full crystallization of the glass. Above the glass transition temperature, the viscosity decreases and the kinetic barrier that prevents crystallization, decreases. If the sample is not heated fast enough, full crystallization of the glass would occur, due to the presence of the Wollastonite fibers. At around 1120 °C, the low-temperature polymorph α-Wollastonite transforms into β-Wollastonite, the high-temperature polymorph.[15] All our observations are done at temperatures above 1300 ° C and, hence, we expect the high-temperature polymorph, β-Wollastonite, to be present. A single CSLM experiment allows observation of growth morphologies and velocities at different undercoolings. As shown in Fig. 7, the temperature is shortly raised to 1420 ° C to melt the crystals again and just before they would fully disappear, the sample is quenched at more than 200 ° C min^{-1} to a different observation temperature.

3. Results and discussion

The crystallization behavior of Wollastonite was observed at 1320 ° C and 1370 °C, which is shown in Figs. 8 and 9, respectively. From these figures, it is clear that there is a remarkable difference in the crystal growth form. This difference was determined to be reproducible in repeated quenching to both observation temperatures. At 1320 °C, Wollastonite is growing dendritically with a sixfold symmetry in the plane of crystallization. The sixfold symmetry is likely a consequence of the crystal structure of the high-temperature polymorph β-Wollastonite, which is reported as monoclinic

Fig. 6. Micrograph from the confocal microscope, showing the Wollastonite fibers on top of the glass at 800 °C. Note the debris at the bottom right, which does not nucleate crystals during the experiment.

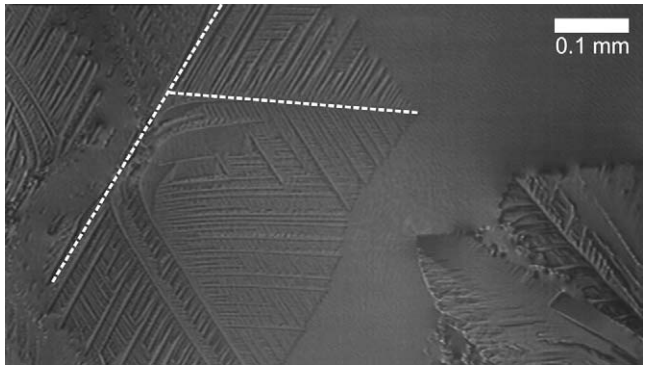

Fig. 8. Micrograph of crystallizing Wollastonite at 1320 ° C in a $42CaO–10Al_2O_3–48SiO_2$ melt. The growth form is clearly dendritic with a hexagonal symmetry.

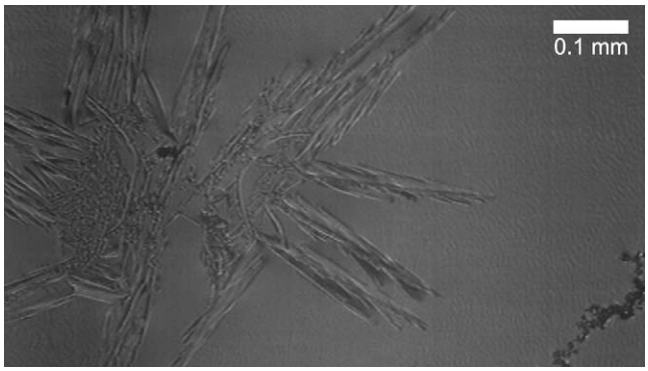

Fig. 9. Micrograph of crystallizing Wollastonite at 1370 ° C in a $42CaO–10Al_2O_3–48SiO_2$ melt. The growth form is faceted. Note the debris at the bottom right, which does not act as a nucleation site during the experiment.

with a pseudo-hexagonal symmetry.[16] In contrast, at 1370 °C, the mineral grows in a faceted manner. It should be noted that both micrographs are recorded in a single experiment, and the growing crystals stem from the same Wollastonite particle.

In the micrographs of Figs. 8 and 9, the laser microscope is focused on a plane that coincides with the liquid–vapor surface. The growing crystals are also in focus and, therefore, we expect the crystallization to occur at the solid–vapor interface. The density of Wollastonite, 2900–3100 kg m^{-3},[17] is slightly higher than the density of the melt, 2690 kg m^{-3} (see Section 3.3). Therefore, the downward buoyancy force is balanced by the surface tension of the liquid.

3.1. Growth forms at 1320 ° C and 1370 °C

The difference in growth form between 1320 ° C (Fig. 8) and 1370 ° C (Fig. 9) can be explained by the Jackson factor,[18] which is a measure for the smoothness of the solid–liquid interface. Faceted crystals have an atomically smooth interface while non-faceted crystals have an atomically rough interface. The Jackson factor is given by:

$$\alpha_J = \xi \frac{\Delta S_f}{R} \quad (1)$$

where ξ is a number expressing the number of broken bonds over the interface, ΔS_f [J mol^{-1} K^{-1}] is the entropy of fusion and R is the ideal gas constant. In general, faceted growth is expected for $\alpha > 2$, while non-faceted growth occurs for $\alpha < 2$. In Eq. (1), ξ is mostly taken 1.

In the classical CALPHAD approach,[19] the Gibbs energy functions in the database are optimized with respect to available experimental data. Previous assessments of the liquid phase in the $CaO–Al_2O_3–SiO_2$ system,[20,21] are based on sparse activity data of CaO and SiO_2 and the phase diagram.[22] We thus expect the entropy of the liquid, in the thermodynamic database of FACTSage,[14] to be less accurate than the entropy of fusion of pure minerals, for which calorimetric experiments exist.[23] Therefore, we calculate the Jackson factor for pure Wollastonite as

$$\alpha_{J,\mathrm{Woll}} = \frac{15.63}{8.31} = 1.88 \quad (2)$$

where the entropy of fusion at the melting point, $\Delta S_f = 15.63$ [J mol^{-1} K^{-1}], is calculated using FACTSage.[14] The value of $\alpha_{J,\mathrm{Woll}}$ is close to the critical value, $\alpha_J = 2$, that separates faceted and non-faceted growth. Furthermore, ΔS_f will increase in the ternary system under study, due to extra entropy of mixing. This is a first indication that a faceted to non-faceted transition should occur for Wollastonite in a ternary silicate melt.

Additionally, the transition from faceted to non-faceted growth form with decreasing temperature can be explained by an increased kinetic undercooling,[24] because the Jackson factor is close to its critical value. Above a certain critical undercooling, the interface roughens and continuous growth, such as dendritic growth, occurs at lower temperatures, whereas faceted growth is observed at higher temperatures (and lower undercoolings). This is a second indication that a faceted to non-faceted transition should occur for Wollastonite in a ternary silicate melt.

The explanation in this Section holds as well for the crystallization experiments in $CaO–Al_2O_3–SiO_2–MgO$ melts of Ref.[4], where Orrling et al. observed dendrites at low temperature and so-called blocky crystals at high temperatures.

3.2. Dendrite tip velocity

For the dendritic growth form at 1320 °C, the tip velocity is measured from the experiment, which is compared with the Ivantsov theory of dendrites.[25] The dendrite tip velocity is determined manually by drawing auxiliary lines on the micrograph at different times (see Fig. 8). A reference line is also drawn to account for possible rotations of the crystal. At every second, the length of the primary dendrite arm, from the reference line to the dendrite tip, is calculated using the correct scaling from the micrograph. Fig. 10 shows the result of the analysis, depicting two dendrite tip positions versus time. The dendrite exhibits a constant velocity, as predicted by theory.[25] Using both linear fits, the dendrite tip velocity is determined as 8.4 ± 0.3 μm s^{-1}.

The micrographs indicate that the observed crystallization occurs at the liquid–vapor interface. Therefore, the crystallization is neither 2D nor 3D. The solute re-distribution can occur downwards to the liquid but towards the vapor, this effect should be negligible. In the following paragraphs, the dendrite tip velocity is compared with theory, for two and three dimensions, to investigate the dimensional growth conditions. It should be noted that more accurate models for growing dendrites exist,[26] but the theory of Ivanstov is sufficient in this work to distinguish the dimensional constraints of the crystal growth.

The dendrite shape in steady-state depends on the growth conditions, more particular the Péclet number $p = \rho v/2D$, where ρ [m] is the dendrite tip radius, v [m s^{-1}] the dendrite tip velocity and D [m^2 s^{-1}] the diffusion coefficient in the liquid. The dendrite shape is assumed to be close to the Ivantsov solution, which relates the Péclet number to the supersaturation, Δ. In

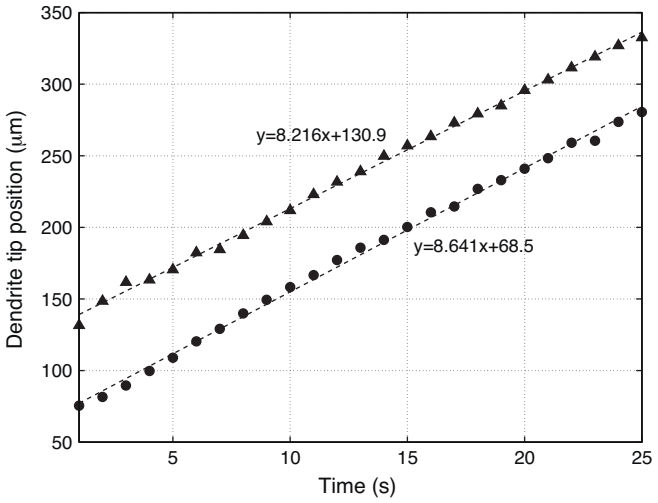

Fig. 10. Dendrite tip position versus time for the dendritic crystallization of Wollastonite at 1320 °C. Two different tip positions are shown and the equations of the linear fit are indicated in the Figure as well. The dendrite tip velocity is thus determined as $8.4 \pm 0.3\ \mu m\ s^{-1}$.

2D, the formula reads:

$$\Delta = \frac{x_L - x_0}{x_L - x_S} = \sqrt{\pi p}\exp(p)\mathrm{erfc}(\sqrt{p}) \tag{3}$$

while in 3D the following formula should be used:

$$\Delta = \frac{x_L - x_0}{x_L - x_S} = p\exp(p)\mathrm{Ei}(p) \tag{4}$$

with Ei(p) the exponential integral $\mathrm{Ei}(p) = \int_{-\infty}^{p}(e^t/t)\,dt$. In both equations, x_L and x_S indicate the equilibrium concentrations, in mole fractions, of the liquid and solid, respectively, at the solid–liquid interface and x_0 is the initial concentration of the liquid. Although the equations above are derived for binary systems, their use is valid in this work because the supersaturation of both independent components, CaO and Al_2O_3, is almost equal for the considered system composition:

$$\Delta_{CaO} = \frac{0.429 - 0.455}{0.429 - 0.500} = 0.366$$
$$\Delta_{Al_2O_3} = \frac{0.095 - 0.060}{0.095 - 0.000} = 0.368 \tag{5}$$

From the Ivantsov formulas in Eqs. (3) and (4), it follows that the theory only relates supersaturation, Δ, to ρv (in the Péclet number p). Therefore, the operating state of the dendrite is an element of an infinite collection of (ρ, v) combinations. However, v is determined experimentally in Fig. 10, which allows us to compare the theoretically predicted radius with the experimentally observed radius. Using $\Delta = 0.37$ in Eqs. (3) and (4), the Péclet number is calculated using Maple™9.5, yielding 0.0442 in 2D and 0.499 in 3D. Furthermore, the diffusion coefficient is estimated at $D = 2 \times 10^{-11}\ m^2\ s^{-1}$ [27,28] and from the experiments, $v = 8.4 \times 10^{-6}\ m\ s^{-1}$. Therefore, the expected dendrite tip radius would be 0.21 μ m in 2D and 2.4 μ m in 3D. Although the resolution of the laser microscope is insufficient for a detailed determination of the experimental radius, it is estimated from the micrographs as 1.0 ± 0.5 μm. It is thus concluded that the growth condition is somewhere between 2D and 3D.

3.3. Validity of the isothermal and mass transport assumptions

The Ivantsov theory in Section 3.2 is only valid for isothermal conditions and diffusion-controlled mass transport around the dendrite tip. In this Section, we therefore calculate the appropriate dimensionless numbers to support both assumptions.

Firstly, in order to assume diffusion-controlled mass transport around the dendrite tip at 1320 °C, the mass transport by convection should be negligible. The tendency for mass transport by thermal convection in the crucible is described by the dimensionless Rayleigh number:

$$\mathrm{Ra} = \frac{g\Delta\rho L^3}{\eta\alpha} \tag{6}$$

where g [$m\ s^{-2}$] is the gravity acceleration, $\Delta\rho$ the difference in density between the hotter and colder melt in the crucible, L [m] a characteristic length of the crucible, η [Pa s] the viscosity of the melt and α [$m^2\ s^{-1}$] the thermal diffusivity. For a worst case scenario, we take the maximum crucible dimension, 4 mm, as the characteristic length and the temperature difference is taken as 30 °C, as shown by the calibration measurements. The thermal diffusivity is calculated as:

$$\alpha = \frac{\lambda}{\rho c_p} = \frac{0.7}{2690 \times 1150} = 2.26 \times 10^{-7} \tag{7}$$

where λ [$W\ m^{-1}\ K^{-1}$] is the thermal conductivity of the melt and c_p [$J\ kg^{-1}\ K^{-1}$] the specific heat capacity of the melt. The thermal conductivity of the melt is taken from Ref.[29]. The density of the melt at 1320 ° C is calculated as $\rho = M/V_m$, with $M = 0.061$ [$kg\ mol^{-1}$] the molar mass of the melt and $V_m = 22.70 \times 10^{-6}$ [$m^3\ mol^{-1}$] the molar volume, calculated from the formulas in Ref.[30]. The specific heat capacity is calculated using FACTSage.[14] The density difference $\Delta\rho$ in Eq. (6) is calculated in a similar way,

$$\Delta\rho = M\left(\frac{1}{V_{m,T_1}} - \frac{1}{V_{m,T_2}}\right) = 0.061\left(\frac{1}{22.70 \times 10^{-6}} - \frac{1}{22.75 \times 10^{-6}}\right) = 5.9 \tag{8}$$

where T_1 and T_2 are respectively 1320 ° C and 1370 °C. The viscosity of the melt is calculated at 1320 ° C by using FACTSage[14] and determined at $\eta = 5.9$ Pa s. The Rayleigh number can now be calculated and, for the presented experiments, $\mathrm{Ra} \approx 3$. This value is well below the critical values (650–1100)[31] above which convection may be expected. We can therefore conclude that mass transport only occurs by diffusion and convection is negligible.

Secondly, for an adequate isothermal experiment, the heat diffusion should be faster than the mass diffusion. The relative

magnitude of these two phenomena is expressed by the Lewis number,

$$\mathrm{Le} = \frac{\alpha}{D} = \frac{2.26 \times 10^{-7}}{2 \times 10^{-11}} \approx 10^{5} \quad (9)$$

where an average diffusion coefficient, D, is calculated using the expressions from Refs.[27,28]. The heat diffusion is thus 5 orders of magnitude faster than mass diffusion and, hence, we can safely assume that the crystal growth occurred under isothermal conditions.

4. Conclusions

We have observed the crystal growth of Wollastonite in a $CaO–Al_2O_3–SiO_2$ melt *in situ* using a high-temperature confocal scanning laser microscope. The crystallization is initiated by seeding the melt with Wollastonite particles, which is an important difference with previous studies of slag crystallization. At high temperature, a faceted growth form is observed, while at low temperature, non-faceted dendrite growth with six-fold anisotropy occurs. Both a decrease in Jackson factor and an increase in kinetic undercooling show that Wollastonite can grow non-faceted at lower temperatures. The dendrite tip velocity is measured and compared with Ivantov's theory for two and three dimensions. In addition to previous studies, the assumptions of isothermal crystallization and diffusion-controlled mass transport are validated by estimating the appropriate dimensionless numbers.

As presented in this work, extensive characterization of the crystallization of silicate melts can be performed through *in situ* observations. Compared to metal solidification, crystallization in the investigated melt is slow and thus, it can be observed in small crucibles and recorded with standard video equipment. The crystal growth form, faceted or non-faceted, and its anisotropy are readily visualized. The small-scale setup ensures an isothermal experiment and diffusion-controlled mass-transport, which allows a quantitative comparison with theory, such as Ivantsov's for dendrites. Moreover, a deeper understanding of the 2D versus 3D character of the growth conditions, could lead to a more quantitative determination of the liquid diffusion coefficient, by using Ivantsov's relation between Péclet number and supersaturation.

Both the mineral, Wollastonite ($CaO{\cdot}SiO_2$), and the melt, $CaO–Al_2O_3–SiO_2$, were chosen because their properties are well-documented and they are feasible to treat in laboratory conditions. Moreover, the $CaO–Al_2O_3–SiO_2$ system is an important basis for many pyrometallurgical and geological processes. The presented technique is, however, not limited to this mineral or melt.

Acknowledgements

JH holds a scholarship from the Agency for Innovation by Science and Technology in Flanders (IWT-SB73161) and NM is a post-doctoral fellow of The Research Foundation – Flanders (FWO). Part of this work has been done in the framework of the bachelor thesis of Anniek Eerdekens. Joris Van Dyck is acknowledged for his technical support for the CSLM apparatus.

References

[1]. Kirkpatrick RJ. Crystal growth from the melt: a review. *American Mineralogist* 1975;**60**:798–814.
[2]. Campforts M, Verscheure K, Boydens E, Van Rompaey T, Blanpain B, Wollants P. On the microstructure of a freeze lining of an industrial nonferrous slag. *Metallurgical and Materials Transactions B* 2007;**38**:841–51.
[3]. Durinck D, Jones PT, Blanpain B, Wollants P, Mertens G, Elsen J. Slag solidification modeling using the Scheil-Gulliver assumptions. *Journal of the American Ceramic Society* 2007;**90**:1177–85.
[4]. Orrling C, Sridhar S, Cramb AW. In situ observation of the role of alumina particles on the crystallization behavior of slags. *ISIJ International* 2000;**40**:877–85.
[5]. McMillan PW. *Glass-ceramics*. Academic Press; 1979.
[6]. Chikarma H, Shibata H, Emi T, Suzuki M. In situ real time observation of planar to cellular and cellular to dendritic transition of crystals growing in Fe-C alloy melts. *Materials Transactions, JIM* 1996;**37**(4): 620–6.
[7]. Jones P, Desmet D, Guo M, Durinck D, Verhaeghe F, Van Dyck J. Using confocal scanning laser microscopy for the in situ study of high-temperature behaviour of complex ceramic materials. *Journal of the European Ceramic Society* 2007;**27**(12):3497–507.
[8]. Rocabois P, Pontoire JN, Lehmann J, Gaye H. Crystallization kinetics of Al_2O_3-CaO-SiO_2 based oxide inclusions. *Journal of Non-Crystalline Solids* 2001;**282**:98–109.
[9]. Valdez M, Prapakorn K, Cramb A, Sridhar S. Dissolution of alumina particles in CaO-Al_2O_3-SiO_2-MgO slags. *Ironmaking & Steelmaking* 2002;**29**:47–52.
[10]. Fox A, Valdez M, Gisby J, Atwood R, Lee P, Sridhar S. Dissolution of ZrO_2, Al_2O_3, MgO and $MgAl_2O_4$ particles in a B_2O_3 containing commercial fluoride-free mould slag. *ISIJ International* 2004;**44**:836–45.
[11]. Liu J, Guo M, Jones PT, Verhaeghe F, Blanpain B, Wollants P. In situ observation of the direct and indirect dissolution of MgO particles in CaO-Al_2O_3-SiO_2-based slag. *Journal of the European Ceramic Society* 2007;**27**:1961–72.
[12]. Park J, Park J, Min D, Lee Y, Kang YB. In situ observation of the dissolution phenomena of SiC particle in CaO-SiO_2-MnO slag. *Journal of the European Ceramic Society* 2010;**30**(15):3181–6.
[13]. Orrling C, Sridhar S, Cramb A. In-situ observations and thermal analysis of crystallization phenomena in mold slags. *High Temperature Materials and Processes* 2001;**20**:195–9.
[14]. Bale CW, Belisle E, Chartrand P, Decterov SA, Eriksson G, Hack K. FactSage thermochemical software and databases – recent developments. *CALPHAD* 2009;**33**:295–311.
[15]. Deer W, Howie R, Zussman J. *Rock-forming minerals: single-chain silicates*. The Geological Society; 1978.
[16]. Yang H, Charles T. On the crystal structure of pseudowollastonite ($CaSiO_3$). *American Mineralogist* 1999;**84**:929–32.
[17]. Roberts W, Rapp G, Cambell T. *Encyclopedia of minerals*. Springer; 1990.
[18]. Jackson J, Hunt J. Transparent compounds that freeze like metals. *Acta Metallurgica* 1965;**13**:1212–5.
[19]. Lukas H, Fries S, Sundman B. *Computational thermodynamics – the calphad method*. Cambrigde University Press; 2007.
[20]. Eriksson G, Pelton A, Critical Evaluation. Optimization of the thermodynamic properties and phase diagrams of the CaO-Al_2O_3, Al_2O_3-SiO_2 and CaO-Al_2O_3-SiO_2 systems. *Metallurgical and Materials Transactions B* 1993;**24**:807–16.
[21]. Mao H, Hillert M, Selleby M, Sundman. Thermodynamic assessment of the CaO-Al_2O_3-SiO_2 system. *Journal of the American Ceramic Society* 2006;**89**:298–308.
[22]. Osborn E, Muan A. *Phase equilibrium diagrams of oxide systems, Plate I. The system CaO-Al_2O_3-SiO_2*. Columbus: Ceramic Foundation; 1960.

[23]. Richet P, Robie R, Hemingway B. Thermodynamic properties of wollastonite, pseudowollastonite and $CaSiO_3$ glass and liquid. *European Journal of Mineralogy* 1991;**3**:475–84.

[24]. Li D, Herlach D. Direct measurements of free crystal growth in deeply undercooled melts of semiconducting materials. *Physical Review Letters* 1996;**77**:1801–4.

[25]. Ivantsov G. *Dokl Akad Naut SSR* 1947;**58**:567.

[26]. Barbieri A, Langer JS. Predictions of dendritic growth rates in the linearized solvability theory. *Physical Review A* 1989;**39**:5314–25.

[27]. Sugawara H, Nagata K, Goto KS. Interdiffusivities matrix of CaO-Al_2O_3-SiO_2 melt at 1723 K to 1823 K. *Metallurgical and Materials Transactions B* 1977;**8B**:605–12.

[28]. Heulens J, Nagata K. Errarum to "Interdiffusivities matrix of CaO-Al_2O_3-SiO_2 melt at 1723 K to 1823 K". *Metallurgical and Materials Transactions B*, in press.

[29]. Kang Y, Morita K. Thermal conductivity of the CaO-Al_2O_3-SiO_2 system. *ISIJ International* 2006;**46**:420–6.

[30]. Courtial P, Dingwell DB. Nonlinear composition dependence of molar volume of melts in the CaO-Al_2O_3-SiO_2 system. *Geochimica et Cosmochimica Acta* 1995;**59**:3685–95.

[31]. Chandrasekhar S. *Hydrodynamic and hydromagnetic stability*. Oxford: Clarendon Press; 1961.